Received: 3 March 2018 | Revised: 27 April 2018 | Accepted: 30 April 2018

DOI: 10.1002/pip.3026

ACCELERATED PUBLICATION

WILEY PROGRESS IN PHOTOVOLTAICS

High-performance low bandgap thin film solar cells for tandem applications

Hossam Elanzeery | Finn Babbe | Michele Melchiorre | Florian Werner | Susanne Siebentritt

Laboratory for Photovoltaics, Physics and Materials Science Research Unit, University of Luxembourg, Belvaux L-4422, Luxembourg

Correspondence
Hossam Elanzeery, Laboratory for Photovoltaics, Physics and Materials Science Research Unit, University of Luxembourg, Belvaux L-4422, Luxembourg.
Email: hossam.elanzeery@gmail.com

Funding information
Luxembourg National Research Fund (FNR)

Abstract

Thin film tandem solar cells provide a promising approach to achieve high efficiencies. These tandem cells require at least a bottom low bandgap and an upper high bandgap solar cell. In this contribution, 2 high-performance $Cu(In,Ga)Se_2$ cells with bandgaps as low as 1.04 and 1.07 eV are presented. These cells have shown certified efficiencies of 15.7% and 16.6% respectively. Measuring these cells under a 780-nm longpass filter, corresponding to the bandgap of a typical top cell in tandem applications (1.57 eV), they achieved efficiencies of 7.9% and 8.3%. Admittance measurements showed no recombination active deep defects. One additional high-performance $CuInSe_2$ thin film solar cell with bandgap of 0.95 eV and efficiency of 14.1% is presented. All 3 cells have the potential to be integrated as bottom low bandgap cells in thin film tandem applications achieving efficiencies around 24% stacked with an efficient high bandgap top cell.

KEYWORDS

admittance steps, deep defects, high-performance solar cells, low bandgap CIGS, quasi-Fermi-level splitting, tandem applications

1 | INTRODUCTION

Currently, there is an increasing demand to provide cheap high-efficiency solar cells that can exceed state-of-the-art single-junction solar cell technologies. One approach to achieve this is through using tandem solar cells. Tandem or multijunction solar cells have the potential to achieve efficiencies of more than 30%.[1,2] Thin film solar cells represent the second generation of photovoltaic technology providing a wide range of possible applications and opportunities to further decrease the cost of solar cells.[3] Thin film tandem cells thus provide a promising approach to obtain high efficiencies at low costs. For thin film tandem cells, different technologies were used focusing on integrating high bandgap solar cells on standard thin film technologies through 2-terminal,[4] 3-terminal,[5] or 4-terminal junctions.[6] Recently, an increasing number of absorber materials with the potential to act as a top higher bandgap cell have been investigated.[7-13] Perovskites have demonstrated the ability to achieve high efficiencies,[10] and because of their high bandgap, they have been implemented as top cells in different tandem configurations using standard bottom cells.[11-13] On the other side, $Cu(In,Ga)Se_2$ (CIGS) is so far the most promising technology for thin film solar cells.[14] Solar cells based on CIGS absorbers have currently achieved the highest efficiency for low-cost thin film PV technologies with a record efficiency of 22.9%.[15] CIGS has been used in tandem applications by stacking individual devices with different bandgap absorbers of CIGS-CdTe,[16] CIGS-dye sensitized,[17] CIGS-CGS,[18] CIGS-CIGS,[19] and recently CIGS-perovskite with efficiencies exceeding 20%.[20,21] The record tandem solar cell based on CI(G)S as a bottom cell[22] reported an

efficiency of 6.0% for CIGS and 4.8% for CIS under a 16.1% perovskite upper high bandgap cell (bandgap of 1.57 eV). In this contribution, we report on the optimization of CIS and CIGS bottom cells, where we introduce promising high-performance solar cells that have the potential to be integrated in tandem devices, with efficiencies of 7.4% to 8.3% for the bottom cell measured under a longpass filter corresponding to the bandgap of the reported perovskite solar cell.[22] One of these cells is a ternary CIS compound that has a lower bandgap compared to CIGS and a less complex structure.[23] The other 2 cells are quaternary CIGS compounds with low Ga content leading to bandgaps of 1.04 and 1.07 eV, which is considerably lower than state-of-the-art CIGS compounds, with efficiencies as high as 15.7% and 16.6% (both certified) respectively. Using the reported 16.1% perovskite top cell,[22] our reported cells have the potential of achieving efficiencies of 23.5% to 24.4% in tandem configuration. We report on the characterization of the 3 high-performance low bandgap cells.

2 | MATERIAL AND METHODS

Polycrystalline CIS and CIGS absorbers were fabricated on molybdenum-coated soda lime glass using a 1-stage coevaporation process for CIS and a 3-stage process for CIGS in a physical vapor deposition tool at substrate temperatures of 530°C. The absorbers were grown targeting a [Cu]/([Ga] + [In]) ratio less than 1 (Cu-poor conditions). Energy-dispersive X-ray spectroscopy (EDX) at an acceleration voltage of 20 kV is used to estimate the elemental average composition of the absorbers. The absorbers showed a [Cu]/[In] ratio of 0.88 for CIS with a bandgap of 0.95 eV, a [Cu]/([In] + [Ga]) ratio of 0.94 for CIGS with a bandgap of 1.04 eV, and 0.91 for CIGS with a bandgap of 1.07 eV. After the absorber growth, the 3 samples were etched in a 5 wt% aqueous solution of potassium cyanide (KCN) for 30 seconds to remove residual oxides.[24] The cells were finished by depositing a chemical bath deposited thin cadmium sulfide (CdS) buffer layer followed by sputtering both window layers: a high resistance ZnO and a biased zinc oxide as a TCO[25] before evaporating contacting nickel/aluminium grids using electron beam evaporation. The biased zinc oxide is a highly conductive nominally undoped ZnO, obtained by means of an additional plasma near the substrate during sputter deposition and is characterized by its high infrared transparency, which makes it particularly useful for low bandgap cells. Details can be found in.[26] Magnesium fluoride (MgF_2) antireflection coating (ARC) layer was deposited at the top of the 3 cells using the same electron beam deposition tool. Each of the 3 substrates is composed of 6 solar cells with areas of approximately 0.5 cm^2, which were defined by mechanical scribing.

Finished solar cells were characterized in current-voltage (*IV*) using a class AAA solar simulator and external quantum efficiency (*EQE*) using chopped illumination from a halogen/xenon lamp and a lock-in amplifier to measure the photocurrent. To extract the activation energy of the dominant recombination channel, current-voltage characteristics as function of temperature (*IVT*) were measured in a temperature range of 320 to 50 K using a closed-cycle helium cryostat. The short-circuit current density (J_{SC}) previously measured in the solar simulator (*IV*) under standard test conditions was used to set the full illumination intensity for the *IVT* measurements. A mechanical shutter was used to allow dark and illuminated measurements within the same experiment. Admittance measurements were performed in the dark, after keeping the sample mounted in the dark at room temperature for 1 night, with an LCR meter using the same cryostat setup. All characterizations were performed after adding the ARC layer. For the extraction of the quasi-Fermi-level splitting (qFLS), photoluminescence (PL) spectra were recorded on CdS-covered absorbers in a home-built calibrated setup at room temperature under continuous monochromatic illumination with 660-nm wavelength.[27,28] The spectral and absolute corrected PL spectra are converted into energy space. In a semilogarithmic plot, the high-energy wing of the PL peak is fitted linearly and is evaluated by means of the simplified Planck's generalized law,[29] providing the qFLS as well as the temperature.

3 | PERFORMANCE AND DEFECT ANALYSIS

Current-voltage measurements were performed on the 3 cells: CIS with a bandgap of 0.95 eV referred to in the text as CIS_0.95, CIGS with a bandgap of 1.04 eV referred to in the text as CIGS_1.04, and CIGS with a bandgap of 1.07 eV referred to in the text as CIGS_1.07. The bandgaps of the 3 cells were determined by linear extrapolation of the long-wavelength slope in the EQE measurements shown below. Two of the 3 cells were sent to Fraunhofer-Institut fur Solare Energiesysteme (ISE) for certification, and their IV characteristics are presented in Figure 1A. Figure 1 A also presents the electrical behavior under light for CIS_0.95 measured in-house. Table 1 summarizes the electrical parameters extracted for the best and an average of 6 solar cells for each of the 3 absorbers. Trends of open-circuit voltage (V_{OC}) deficit and short-circuit current density (J_{SC}) as a function of absorber bandgap are shown in Figure 2. All IV measurements were performed after adding an ARC layer.

In Figure 1A, it is observed that V_{OC} increases and J_{SC} decreases with increasing bandgap. To better compare the different cells with different bandgaps, the V_{OC} deficit ($V_{OC.def}$) was calculated for each of the 3 cells from the difference between their bandgap energies (E_G) and their corresponding V_{OC} as in Equation 1. Furthermore, the electrical efficiency (η_{el}) was calculated as the ratio between V_{OC} times fill factor (FF) of each cell to the Shockley-Queisser (*SQ*)[30] limit for V_{OC} times FF at the corresponding bandgap of each cell as in Equation 2. The optical efficiency (η_{op}) was calculated as the ratio between the J_{SC} of each cell to the SQ limit for J_{SC} at the corresponding bandgap as in Equation 3[31]:

$$V_{OC.def} = \frac{1}{q}E_G - V_{OC}, \tag{1}$$

$$\eta_{el} = \frac{V_{OC}{}^{*}FF}{V_{OC}^{SQ}{}^{*}FF^{SQ}}, \tag{2}$$

$$\eta_{op} = \frac{J_{SC}}{J_{SC}^{SQ}}, \tag{3}$$

where $V_{OC}{}^{SQ}$ is the SQ limit for V_{OC} with values of 705, 789, and 817 mV, FF^{SQ} is the SQ limit for FF with values of 0.88, 0.88, and 0.89, $J_{SC}{}^{SQ}$ is the SQ limit for J_{SC} with values of 50.9, 46.1, and 44.7 mA/cm^2 for bandgaps of 0.95, 1.04, and 1.07 eV respectively, calculated with an AM1.5 spectrum.[32] Based on the calculated efficiencies

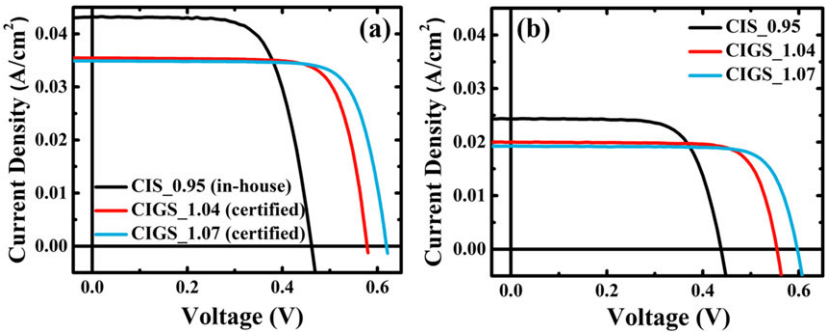

FIGURE 1 IV characteristics of (A) CIS_0.95 measured in-house and CIGS_1.04 and CIGS_1.07 measured in Fraunhofer-ISE and (B) CIS_0.95, CIGS_1.04, and CIGS_1.07 measured under a longpass optical filter with a cutoff wavelength of 780 nm. All measurements were performed after adding an ARC layer. The scales of both figures are the same [Colour figure can be viewed at wileyonlinelibrary.com]

TABLE 1 IV parameters for the best solar cell for CIS_0.95, CIGS_1.04, and CIGS_1.07, measured in-house under standard test conditions as well as for CIGS_1.04 and CIGS_1.07 certified by Fraunhofer-ISE

Sample	Efficiency (%)	FF (%)	V_{OC} (mV)	J_{SC} (mA/cm^2)	$V_{OC.def}$ (mV)	η_{el} (%)	η_{op} (%)	qFLS (meV)
CIS_0.95 (in-house)	14.1 (13.2)	70.6 (68.3)	462 (462)	43.2 (41.8)	488	53	85	494
CIGS_1.04 (in-house)	17.3 (16.1)	77.5 (75.1)	577 (575)	38.7 (37.3)	463	64	84	633
CIGS_1.07 (in-house)	18.3 (17.3)	78.9 (77.9)	621 (617)	37.3 (36.0)	449	66	83	674
CIGS_1.04 (certified)	15.7	76.6	578	35.4	462	64	77	-
CIGS_1.07 (certified)	16.6	76.9	619	34.9	451	66	78	-

Values in brackets represent the average of 6 solar cells on each sample. The V_{OC} deficit and electrical and optical efficiency are calculated as reported.[31] The last column displays the quasi-Fermi-level splitting of the absorbers covered with CdS at 1-sun equivalent illumination

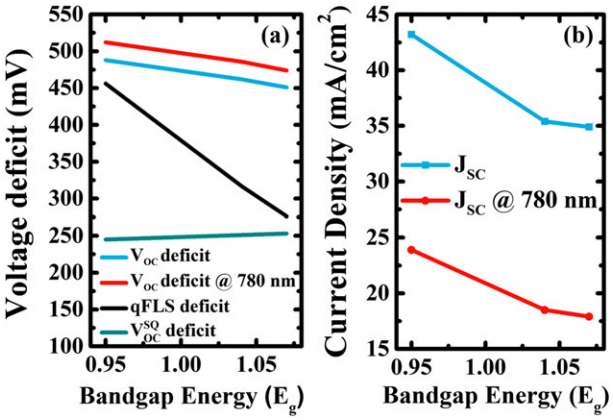

FIGURE 2 A, V_{OC} deficit, V_{OC} deficit with a longpass filter at a wavelength of 780 nm, V_{OC}^{SQ} deficit, and qFLS deficit. B, J_{SC} and J_{SC} with a longpass filter at a wavelength of 780 nm as function of bandgap energy (E_g) for CIS_0.95 (in-house), CIGS_1.04 (certified), and CIGS_1.07 (certified) [Colour figure can be viewed at wileyonlinelibrary.com]

summarized in Table 1, it can be concluded that the cells lose more in recombination than in incomplete absorption ($\eta_{el} < \eta_{op}$). Moreover, the V_{OC} deficit decreases and electrical efficiency increases with the addition of Ga as presented in Table 1 and shown in Figure 2A, indicating reduced recombination. It is likely that the main effect of Ga addition is a gradient with increasing band gap toward the back contact, as usually observed in Cu(In,Ga)Se_2 cells prepared by the 3-stage process, and which prevents back contact recombination.[33] The V_{OC}^{SQ} deficit is also plotted in Figure 2A, which corresponds to the difference between the bandgap and the *SQ* V_{OC} limit with values of 245, 251, and 253 mV for bandgaps of 0.95, 1.04, and 1.07 eV respectively. To verify whether the improved recombination properties with Ga are intrinsic to the absorber, or occur when processing the finished solar cell, we determine the qFLS of the different absorbers covered only with CdS. The qFLS at the equivalent illumination of 1 sun is obtained from calibrated PL measurements at room temperature, and has values of 494, 633, and 674 meV for the 3 cells respectively. The difference between the qFLS and the SQ limit V_{OC}^{SQ} is reduced from 211 to 156 to 143 meV (difference between V_{OC}^{SQ} and V_{OC} = 243, 212, and 196 mV) with the addition of Ga, but it is still quite high. Moreover, the difference between the bandgap and the qFLS for the 3 cells referred to as the qFLS deficit is reduced significantly from 456 to 317 to 276 meV with the addition of Ga as presented in Figure 2A. Accordingly, the better electronic performance of the Ga containing solar cells is indeed at least partially linked to a better electronic quality of the absorber itself, but further optimization of the buffer/window stack still promises further efficiency potential.

The electrical parameters of the 2 certified cells are also presented in Table 1. Table 1 indicates an excellent match between the certified samples and the in-house measured ones in V_{OC} and FF. However, the J_{SC} measured in-house is overestimated as it is measured without spectral correction. The certified J_{SC} for CIGS_1.04 has a value of 35.4 mA/cm^2 leading to an efficiency of 15.7%. For CIGS_1.07, a certified J_{SC} of 34.9 mA/cm^2 leads to an efficiency of 16.6%. The certified values prove the high performance of the fabricated cells, showing efficiencies around 16% for bandgaps as low as 1.04 eV. Moreover, the FF increases for CIGS_1.04 and CIGS_1.07 compared to CIS_0.95.

Targeting tandem applications, a longpass filter of 780 nm (1.59 eV photon energy) was used, corresponding to the bandgap (1.57 eV) of a perovskite top cell in a state-of-the-art thin film tandem solar cell reported.[22] The IV characteristics measured under this filter for the 3 low bandgap cells are presented in Figure 1B. The filter acts in place of the upper high bandgap cell in tandem applications. The measured J_{SC} under the longpass filter was then divided by a factor

TABLE 2 IV parameters for the best solar cell for CIS_0.95, CIGS_1.04, and CIGS_1.07, measured in-house under a longpass optical filter of a wavelength of 780 nm

Sample with an Optical Filter of 780 nm	Efficiency (%)	FF (%)	V_{OC} (mV)	J_{SC} (mA/cm^2)
CIS_0.95	7.4	71.0	438	23.9
CIGS_1.04	7.9	77.0	554	18.5
CIGS_1.07	8.3	78.0	596	17.9

corresponding to the ratio between the measured J_{SC} under standard conditions and the certified one to correct for the spectral mismatch in our in-house setup. The IV parameters for the 3 cells are presented in Table 2. The 3 cells achieved efficiencies of 7.4% to 8.3%, more than the CI(G)S cells (4.8%-6%) reported as bottom low bandgap cells in the 22.1% record perovskite/CIGS devices.[22] Our cells also show comparable bandgaps and promising potentials of efficiencies up to 24.4% for tandem applications. Figure 2 summarizes the V_{OC} deficit measured with full spectrum, V_{OC} deficit measured with the optical filter at a wavelength of 780 nm, V_{OC}^{SQ} deficit, and qFLS deficit (Figure 2A), as well as J_{SC} measured with full spectrum and with the same optical filter (Figure 2B), as function of bandgap energy.

Reflection measurements were performed for each of 3 low bandgap solar cells. Based on the reflection measurements, a tailored MgF_2 ARC layer was deposited for each cell separately. The thickness of the ARC layer corresponds to the wavelength of the highest reflection maxima from reflection measurements.[34] Figure 3 represents the certified EQE spectra for CIGS_1.04 and CIGS_1.07 measured at Fraunhofer-ISE Labs as well as for CIS_0.95 measured in-house after adding the ARC layer for the 3 cells. The certified EQE measurements are in an excellent agreement with the ones measured in-house (not shown here). High EQE values very close to 100% were achieved for the targeted wavelength region. The QE in the short wavelength region for CIGS_1.04 and CIGS_1.07 is lower than that of CIS_0.95 because of a thicker CdS layer that has been deposited for longer durations for these 2 cells. CIS_0.95 retains a high EQE up to long wavelengths because a biased ZnO layer was used as transparent conductive oxide (TCO), which has a high transparency in this spectral

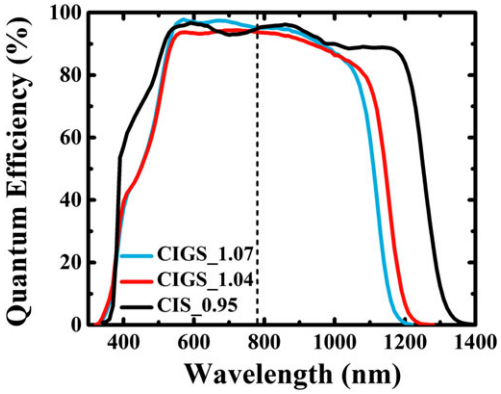

FIGURE 3 EQE measurements for CIS_0.95 measured in-house under standard test conditions, CIGS_1.04 and CIGS_1.07 measured at Fraunhofer-ISE Labs. All measurements were performed after adding an ARC layer. The short dashed line represents the 780-nm wavelength corresponding to the bandgap of the state-of-the-art top cell[22] [Colour figure can be viewed at wileyonlinelibrary.com]

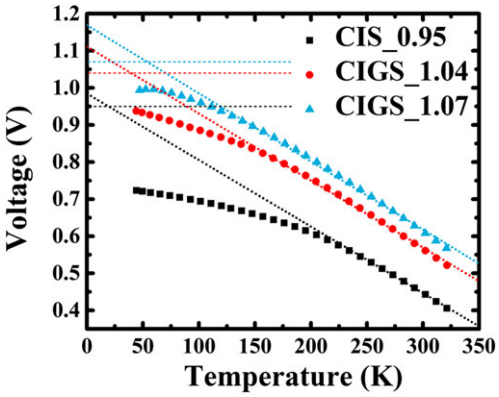

FIGURE 4 Temperature dependence of the open circuit voltage for CIS_0.95 (black), CIGS_1.04 (red), and CIGS_1.07 (blue). A linear fit at high temperatures (short dotted line) is used to extract the activation energy at 0 K. The short dashed line represents the bandgap energy for CIS_0.95 (black), CIGS_1.04 (red), and CIGS_1.07 (blue) [Colour figure can be viewed at wileyonlinelibrary.com]

region because of low free-carrier absorption.[25] IVT measurements between 320 to 50 K were performed under light conditions for the 3 cells to identify the dominant recombination path in these cells. The activation energy given by the open-circuit voltage extrapolated to 0 K is comparable to the bandgap for each cell as shown in Figure 4, indicating that the dominant recombination path is in the bulk of these absorbers.[35] The extrapolated activation energies at 0 K show slightly higher values compared to the bandgap extracted from EQE because of an expected 75 meV additional activation energy accounting for the temperature-dependent thermal velocity and effective density of states indicated in[36] and reported in[37] as well. To identify the defects present in these cells, admittance measurements at 0 V bias voltage were performed in the dark after keeping the samples in the dark at room temperature overnight.

Figure 5A to C shows the temperature-dependent capacitance spectra for CIS_0.95, CIGS_1.04, and CIGS_1.07 respectively. From these figures, it can be deduced that there are 3 capacitance features for each cell, which are marked in Figure 5A. At high temperatures (step 1), we observe a broad capacitance dispersion, which might be related to tail states or in-homogeneities.[38] Alternatively, such a dispersion might indicate the presence of a broad defect-related capacitance step at frequencies well below our measurement range. In that case, the low inflection frequency well below 100 Hz, and correspondingly long characteristic lifetime, suggests only a weak recombination activity even at room temperature. At the lowest temperatures (step 3), we observe a mobility or carrier freeze-out (with an activation energy of 50-60 meV for the 3 cells), because the capacitance drops to the geometrical capacitance of the absorber of approximately 5 nF/cm^2.

If significant recombination-active deep defects were present within the absorber, these defects would need to correspond to step 2 at intermediate temperatures. The inflection frequencies of the capacitance spectrum corresponding to step 2, scaled by T^{-2},[39] are plotted in an Arrhenius plot presented in Figure 5D to F. From the slope of the Arrhenius plot, the activation energy of the midtemperature admittance step (step 2) was deduced. The activation energy for CIGS_1.04 is around 115 meV and CIGS_1.07 is close to 90 meV. For CIS_0.95, a double step could be observed with activation energies of 40 and

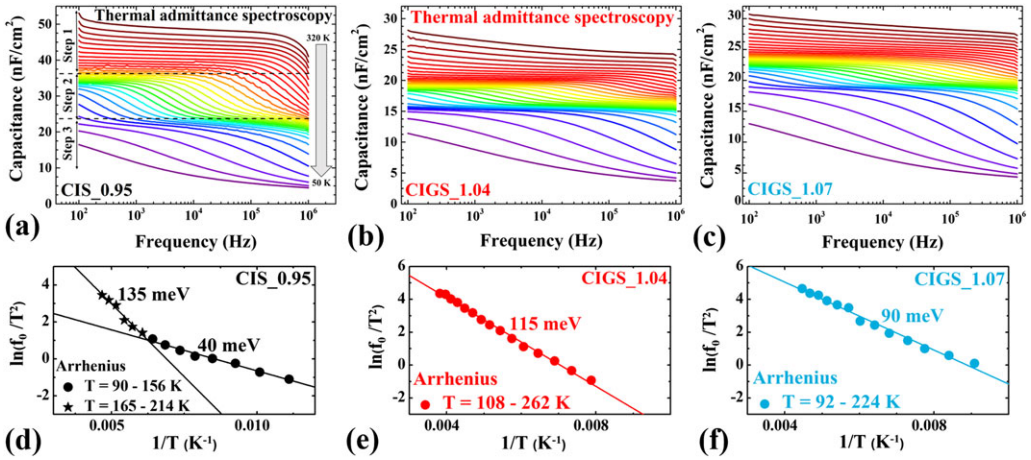

FIGURE 5 Temperature-dependent capacitance spectra for (A) CIS_0.95, (B) CIGS_1.04, and (C) CIGS_1.07, and corresponding Arrhenius plots for (D) CIS_0.95, (E) CIGS_1.04, and (F) CIGS_1.07 [Colour figure can be viewed at wileyonlinelibrary.com]

135 meV. To confirm whether this capacitance step is indeed related to a defect signature or a barrier, the extracted activation energies were compared to the temperature dependences of series resistance and dark diode current from IVT measurements.[40,41]

The series resistance is virtually constant with respect to temperature and thus cannot explain the second capacitance step. The forward-bias dark current densities were found to follow a simple diode model without signatures for interface barriers for all 3 devices. This indicates that the main admittance step is not related to a barrier[41] but to shallow defects. Based on the activation energies of step 2, it can be observed that the activation energy of the main capacitance step decreases from 135 to 115 to 90 meV with the addition of Ga. This energy is in the range of the energies of 3 shallow acceptors observed by PL.[42-44] Accordingly, we attribute the second capacitance step to shallow dopant defects and find that the capacitance spectra of all 3 devices do not show any obvious signatures of efficient recombination active deep defects.

4 | CONCLUSION

Two CIGS high-performance solar cells with bandgaps as low as 1.04 and 1.07 eV were presented. These CIGS solar cells have V_{OC} of 578 and 619 mV, FF of 76.6 and 76.9% with J_{SC} of 35.4 and 34.9 mA/cm^2, leading to certified efficiencies of 15.7% and 16.6% for bandgaps of 1.04 and 1.07 respectively. These cells are promising candidates for the bottom cell in tandem applications. Recently, a similar result of 16.1% efficiency (in-house measurements) was presented with a band gap of 1.0 eV.[37] Our certified 16.6% efficiency is at the moment the best low bandgap cell reported. Using a longpass filter of 780 nm (corresponding to a bandgap of 1.59 eV for a high bandgap top cell), these CIGS cells achieve efficiencies of 7.9% and 8.3% respectively. No deep recombination active defects can be revealed from admittance measurements. One more high-performance solar cell with an even lower band gap was also presented. A CIS cell with a bandgap of 0.95 eV and an efficiency of 14.1%. The 3 cells have the potential to achieve high efficiencies (23.5%-24.4%) in combination with an efficient high bandgap top cell.[22]

ACKNOWLEDGEMENT

This contribution has been funded by Luxembourg National Research Fund (FNR) in the framework of the CURI-K and SURPASS projects, which are gratefully acknowledged.

ORCID

Hossam Elanzeery http://orcid.org/0000-0001-6032-2499
Finn Babbe http://orcid.org/0000-0002-9131-638X
Florian Werner http://orcid.org/0000-0001-6901-8901

REFERENCES

1. Coutts TJ, Emery KA, Ward JS. Modeled performance of polycrystalline thin-film tandem solar cells. *Prog In Photovoltaics: Research and Applications*. 2002;10(3):195-203.
2. Coutts TJ, Ward JS, Young DL, Emery KA, Gessert TA, Noufi R. Critical issues in the design of Polycrystalline, thin-film tandem solar cells. *Prog in Photovoltaics: Research and Applications*. 2003;11(6):359-375.
3. Green MA. Consolidation of thin-film photovoltaic technology: The coming decade of opportunity. *Prog in Photovoltaics: Research and Applications*. 2006;14(5):383-392.
4. Kwon J, Im MJ, Kim CU, et al. Two-terminal DSSC/silicon tandem solar cells exceeding 18% efficiency. *Energ Environ Sci*. 2016;9(12):3657-3665.
5. Sista S, Hong Z, Park M-H, Xu Z, Yang Y. High-efficiency polymer tandem solar cells with three-terminal structure. *Comm Adv Energy Materials*. 2010;22(8):E77-E80.
6. Werner J, Barraud L, Walter A, et al. Efficient near-infrared-transparent perovskite solar cells enabling direct comparison of 4-terminal and monolithic Perovskite/silicon tandem cells. *ACS Energy Lett*. 2016;1(2):474-480.
7. Elanzeery H, Buffière M, Messaoud KB, et al. Multistep deposition of $Cu_2Si(S,Se)_3$ and $Cu_2ZnSiSe_4$ high band gap absorber materials for thin film solar cells. *Physica Status Solid: Rapid Research Letters*. 2015;9(6):338-343.
8. Buffière M, Elanzeery H, Oueslati S, et al. Physical characterization of $Cu_2ZnGeSe_4$ thin films from annealing of Cu–Zn–Ge precursor layers. *Thin Solid Films*. 2015;582:171-175.
9. Brammertz G, Vermang B, Elanzeery H, et al. Fabrication of ternary and quaternary chalcogenide compounds based on Cu, Zn, Sn and Si for thin film photovoltaic applications. *Physica Status Solidi C*. 2017;14:6.

10. Yang S, Fu W, Zhang Z, Chena H, Li C-Z. Recent advances in perovskite solar cells: Efficiency, stability and lead-free perovskite. *J Mater Chem A*. 2017;5(23):11462-11482.
11. Jaysankar M, Qiu W, Eerden MV, et al. Four terminal perovskite/silicon multijunction solar modules. *Advanced Energy Materials*. 2017;7(15).
12. Rühle S. The detailed balance limit of perovskite/silicon and perovskite/CdTe tandem solar cells. *Physica Status Solidi a*. 2017;214(5).
13. https://www.pv-magazine.com/2017/08/08/imec-hits-23-9-efficiency-on-4cm-tandem-perovskitesilicon-module.
14. Lee TD, Ebong AU. A review of thin film solar cell technologies and challenges. *Renew Sustain Energy Rev*. 2017;70:1286-1297.
15. https://www.pv-magazine.com/2017/12/20/solar-frontier-hits-new-thin-film-cell-efficiency-record/
16. M. Symko-Davies and R. Noufi, *Proc. of 20th European Photovoltaic Solar Energy Conference* (WIP-Renewable Energies, Munich, Germany) 2005.
17. Liska P, Thampi KR, Grätzel M, et al. Nanocrystalline dye-sensitized solar cell/copper indium gallium selenide thin-film tandem showing greater than 15% conversion efficiency. *Appl Phys Lett*. 2006;88(20):203103.
18. Nishiwaki S, Siebentritt S, Walk P. A stacked chalcopyrite thin-film tandem solar cell with 1.2 V open-circuit voltage. *Progress in Photovoltaics*. 2003;11(4):243-248.
19. Kaigawa R, Funahashi K, Fujie R, et al. Tandem solar cells with Cu(In,Ga)S_2 top cells on ZnO coated substrates. *Solar Energy Materials & Solar Cells*. 2010;94(11):1880-1883.
20. Guchhait A, Dewi HA, Leow SW, et al. Over 20% efficient CIGS-perovskite tandem solar cells. *ACS Energy Letters*. 2017;2(4):807-812.
21. Kranz L, Abate A, Feurer T, et al. High-efficiency polycrystalline thin film tandem solar cells. *J Phys Chem Lett*. 2015;6(14):2676-2681.
22. Fu F, Feurer T, Weiss TP, et al. High-efficiency inverted semi-transparent planar perovskite solar cells in substrate configuration. *Nature Energy*. 2016;2(1):16190.
23. AbuShama J, Noufi R, Johnston S, Ward S, Wu X. Improved performance in CuInSe2 and surface-modified CuGaSe2 solar cells. *proceedings 31st IEEE Photovoltaic Specialists Conference*. 2005;299-302.
24. Regesch D, Gütay L, Larsen JK, et al. Degradation and passivation of $CuInSe_2$. *Appl Phys Lett*. 2012;101(11):112108.
25. Hala M, Kato H, Algasinger M, et al. Improved environmental stability of highly conductive nominally undoped ZnO layers suitable for n-type windows in thin film solar cells. *Solar Energy Materials & Solar Cells*. 2017;161:232-239.
26. Hala M, Fujii S, Redinger A, et al. *Progress in Photovoltaic Research Application*. 2015;23(11):1630.
27. Unold T, Gütay L. Photoluminescence analysis of thin-film solar cells. In: Abou-Ras D, Kirchartz T, Rau U, eds. *Advanced Characterization Techniques for Thin Film Solar Cells*. Weinheim, Germany: Wiley-VCH Verlag GmbH & Co. KGaA; 2011:151-175.
28. Babbe F, Choubrac L, Siebentritt S. Quasi Fermi level splitting of Cu-rich and Cu-poor Cu(In,Ga)Se_2 absorber layers. *Appl Phys Lett*. 2016;109:8, 82105.
29. Würfel P. The chemical potential of radiation. *J Physics C Solid State Physics*. 1982;15(18):3967-3985.
30. Shockley W, Queisser HJ. Detailed balance limit of efficiency of p-n junction solar cells. *J Appl Phys*. 1961;32(3):510-519.
31. Polman A, Knight M, Garnett EC, Ehrler B, Sinke WC. Photovoltaic materials: Present efficiencies and future challenges. *Science*. 2016;352(6283):aad4424.
32. Siebentritt S. What limits the efficiency of chalcopyrite solar cells? *Sol Energy Mater Sol Cells*. 2011;95(6):1471-1476.
33. Dullweber T, Lundberg O, Malmstrom J, et al. Back surface band gap gradings in Cu(In,Ga)Se_2 solar cells. *Thin Solid Films*. 2001;387(1-2):11-13.
34. Messaoud KB, Brammertz G, Buffière M, et al. Modelling of $Cu_2ZnSnSe_4$-CdS-ZnO thin film solar cell. *Materials Research Express*. 2017;4(11).
35. Scheer R, Schock H-W. *Chalcogenide photovoltaics: Physics, technologies, and thin film devices*. Boschstr. 12, 69469 Weinheim, Germany: Wiley-VCH Verlag GmbH & Co. KGaA; 2011.
36. Hölscher T, Förster S, Schneider T, Maiberg M, Widdra W, Scheer R. Light induced degradation of Cu(In,Ga)Se_2 thin film surfaces. *Appl Phys Lett*. 2017;111(1):011604.
37. Feurer T, Bissig B, Weiss TP, et al. Single-graded CIGS with narrow bandgap for tandem solar cells. *Science and Technology of Advanced Materials*. 2018;19(1):263-270.
38. Hirschorn B, Orazem ME, Tribollet B, Vivier V, Frateur I, Musiani M. Determination of effective capacitance and film thickness from constant-phase-element parameters. *Electrochim Acta*. 2010;55(21):6218-6227.
39. Blood P, Orton JW. *The electrical characterization of semiconductors: Majority carriers and electron states*. London: Academic Press; 1992.
40. Weiss TP, Redinger A, Luckas J, Mousel M, Siebentritt S. Admittance spectroscopy in kesterite solar cells: Defect signal or circuit response. *Appl Phys Lett*. 2013;102(20):202105.
41. Werner F, Wolter MH, Siebentritt S, et al. Alkali treatments of Cu(In,Ga)Se_2 thin-film absorbers and their impact on transport barriers. https://doi.org/10.1002/pip.3032
42. Siebentritt S, Rega N, Zajogin A, Lux-Steiner MC. Do we really need another PL study of $CuInSe_2$? *phys stat sol*. 2004;1(9):2304-2310.
43. Bauknecht A, Siebentritt S, Albert J, Lux-Steiner MC. Radiative recombination via intrinsic defects in $Cu_xGa_ySe_2$. *J Appl Phys*. 2001;89(8):4391-4400.
44. Siebentritt S, Rau U. *Wide-gap chalcopyrites*. Berlin, Heidelberg: Springer; 2006:113-156.

How to cite this article: Elanzeery H, Babbe F, Melchiorre M, Werner F, Siebentritt S. High-performance low bandgap thin film solar cells for tandem applications. *Prog Photovolt Res Appl*. 2018;1–6. https://doi.org/10.1002/pip.3026